Journal of Physics: Conference Series

The response of a high-speed train wheel to a harmonic wheel-rail force

To cite this article: Xiaozhen Sheng *et al* 2016 *J. Phys.: Conf. Ser.* **744** 012145

The response of a high-speed train wheel to a harmonic wheel-rail force

Xiaozhen Sheng, Yuxia Liu, Xin Zhou
State Key Laboratory of Traction Power, Southwest Jiaotong University, Chengdu 610031, China

E-mail:shengxiaozhen@hotmail.com

Abstract. The maximum speed of China's high-speed trains currently is 300km/h and expected to increase to 350-400km/h. As a wheel travels along the rail at such a high speed, it is subject to a force rotating at the same speed along its periphery. This fast moving force contains not only the axle load component, but also many components of high frequencies generated from wheel-rail interactions. Rotation of the wheel also introduces centrifugal and gyroscopic effects. How the wheel responds is fundamental to many issues, including wheel-rail contact, traction, wear and noise. In this paper, by making use of its axial symmetry, a special finite element scheme is developed for responses of a train wheel subject to a vertical and harmonic wheel-rail force. This FE scheme only requires a 2D mesh over a cross-section containing the wheel axis but includes all the effects induced by wheel rotation. Nodal displacements, as a periodic function of the cross-section angle θ, can be decomposed, using Fourier series, into a number of components at different circumferential orders. The derived FE equation is solved for each circumferential order. The sum of responses at all circumferential orders gives the actual response of the wheel.

1. Introduction

Nowadays more and more countries are building, extending, or planning to develop, high-speed railway networks. In China, more than 19000km high-speed railways are already in operation at a maximum speed of 300km/h. By high-speed train it takes about 5 hours from Shanghai to Beijing, but travellers are still feeling too long. Train speeds are expected to increase even higher, e.g. to 350-400km/h, to suit for big countries such as China and Russia, and to gain competition advantages over airways.

As a wheel travels along the rail at such a high speed, it is subject to a force moving at the same speed along its periphery. This fast moving force contains not only a static component, i.e. the axle load, but also many components of high frequencies generated from wheel-rail interactions. The rotation of the wheel also introduces centrifugal and gyroscopic effects. It can be expected that the dynamics of a rotating wheel is much more complicated than that of a non-rotating wheel.

Issues concerning the railway industry, such as generation and radiation of rail-wheel rolling noise, initiation and growth of rail-wheel roughness, rail corrugation and wheel out-of-round, are fundamentally the result of wheel-rail interactions of high frequency. When dealing with wheel-rail high-frequency interactions in the frequency domain, the receptance of the wheel at the wheel-rail contact point is normally required. Most of researchers compute the receptance from a stationary wheel without any rotation, even treat the wheel as a rigid body, and only few researchers have taken into account the rotation of the wheel but with some sorts of simplification.

In References [1, 2], Thompson et al replace the rotation of the wheel with a rotating load. This simplification enables the use of the modal superposition method to construct the response of the wheel to a moving load. The normal modes are computed using the finite element (FE) method for the wheel being at stationary and the wheel centre being fixed, with all the structural effect of rotation, such as centrifugal stiffening or softening and Coriolis forces, being excluded.

Reference [3] presents a technique for analysing the structural vibrations of a solid of revolution rotating about its main axis. The method is based on two treatments: 1) the displacement of the solid is split into two parts, one associated with the rigid motion of the solid (that is the rotation about the main axis) and the other associated with the deformation of the solid; 2) any deformed shape of the solid can be calculated as a linear combination of its non-rotating modes. It can be seen in the paper that, the axis of rotation is fixed. This technique is applied in Reference [4] to model a rotating flexible wheelset which is coupled with a flexible track model and a non-Hertzian/non-steady contact model to investigate rail corrugation initiation, although in dealing with wheel-rail interaction, allowing the axis of rotation to vibrate vertically is essential.

This paper offers an alternative approach to modelling the dynamic response of a spinning solid of revolution, in particular a railway wheel. At the moment the axis of rotation is allowed to vibrate vertically only. By making use of its axial symmetry, a special finite element scheme, combined with application of the momentum law to the wheel, is developed for responses of a train wheel subject to a vertical and harmonic wheel-rail force. This FE scheme only requires a 2D mesh over a cross-section containing the wheel axis but includes all the effects induced by wheel rotation. Unknowns include vertical displacement of the wheel axis, and nodal displacements, as a function of the cross-section angle θ, of the cross-section observed from the rotating wheel. Since the nodal displacements are a periodic function of θ, they can be decomposed, using Fourier series, into a number of components at different circumferential orders. The derived FE equation is solved for each circumferential order. The sum of responses at all circumferential orders gives the actual response of the wheel observed from the rotating wheel.

The development of the FEM equation is presented in Section 2. Section 3 is devoted to a more specific situation, the response of a rotating wheel to a vertical harmonic wheel-rail force which is stationary if observed from the train but rotating if from the wheel. Some example results and discussions are presented in Section 4. Conclusions are summarised in Section 5.

2. Differential equations of motion

2.1. Coordinate systems

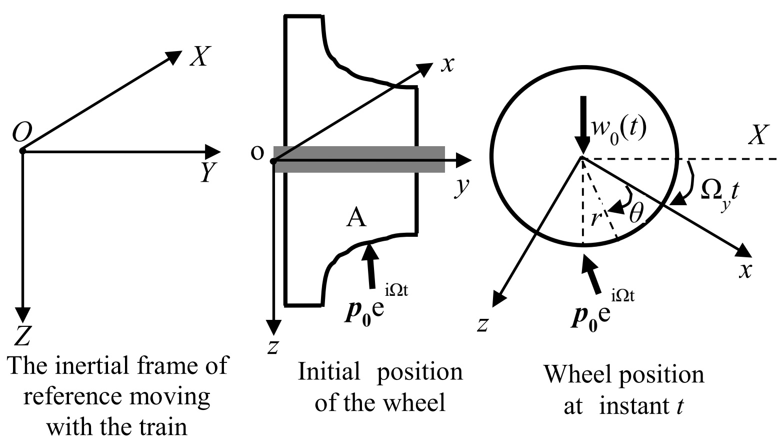

Figure 1. Coordinate systems.

As shown in Figure 1, coordinate system *oxyz* is rigidly attached on the wheel with the *y*-axis coincides with the wheel axis. It rotates uniformly about the *y*-axis at the wheel rotation speed Ω_y in the direction shown. Observed from an inertial frame of reference, *OXYZ*, which moves uniformly with the train in the track direction, the *y*-axis is allowed to vibrate in the vertical direction only, and the vibrational displacement is denoted by $w_0(t)$, directed downwards.

A point defined by coordinates (*x*, *y*, *z*) with respect to *oxyz*, may be expressed alternatively using cylindrical coordinates (*r*, *y*, θ), where $r=(x^2+z^2)^{1/2}$, and $x=r\cos\theta$, $z=r\sin\theta$. Angle θ defines a cross-section of the wheel which contains that point and the *y*-axis, see Figure 1. This cross-section is termed the θ-plane.

2.2. Definition of nodal displacements of an element

Two-dimensional finite elements are created on the θ-plane (Figure 2). The same discretisation is also made on the θ+dθ -plane. An element on the θ-plane and its counterpart on the θ+dθ -plane define an element volume. Nodal displacements, observed from *oxyz*, of an element on the θ-plane are denoted by a 3*n* vector.

$$\boldsymbol{q}(\theta,t)=(u_1,\upsilon_1,w_1,u_2,\upsilon_2,w_2,\cdots,u_n,\upsilon_n,w_n)^{\mathrm{T}}, \tag{1}$$

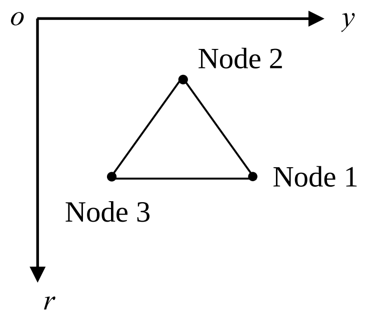

Figure 2. An finite element on the θ-plane.

where, *n* is the number of nodes, and u,υ,w are displacement components in the *r*- (radial), *y*- (axial) and θ- (circumferential) directions. The corresponding externally applied nodal force vector is denoted by $\boldsymbol{f}_0(\theta,t)$, which is of order $3n\times1$. The units of a nodal force are N/rad. The area of the element is denoted by *A*.

A shape function matrix of order $3\times3n$ is defined and denoted by $\boldsymbol{\Phi}(r,y)$, so that the displacements of the element at any point within the element may be approximated as $\boldsymbol{v}(r,y,\theta,t)=\boldsymbol{\Phi}(r,y)\boldsymbol{q}(\theta,t)$, and the velocity vector at (*r*, *y*, θ) is given by

$$\dot{\boldsymbol{v}}(r,y,\theta,t)=(\dot{u}(r,y,\theta,t),\dot{\upsilon}(r,y,\theta,t),\dot{w}(r,y,\theta,t))^{\mathrm{T}}=\boldsymbol{\Phi}(r,y)\dot{\boldsymbol{q}}(\theta,t). \tag{2}$$

2.3. Kinetic and potential energy of the element volume

The kinetic energy of the element volume, observed from the *oxyz* system, is given by

$$\begin{aligned} T&=\frac{1}{2}\int_A\rho(\dot{\boldsymbol{v}}(r,y,\theta,t))^{\mathrm{T}}(\dot{\boldsymbol{v}}(r,y,\theta,t))r\mathrm{d}A\mathrm{d}\theta \\ &=\frac{1}{2}(\dot{\boldsymbol{q}}(\theta,t))^{\mathrm{T}}\left(\int_A\rho r(\boldsymbol{\Phi}(r,y))^{\mathrm{T}}(\boldsymbol{\Phi}(r,y))\mathrm{d}A\right)\dot{\boldsymbol{q}}(\theta,t)\mathrm{d}\theta, \\ &=\frac{1}{2}(\dot{\boldsymbol{q}}(\theta,t))^{\mathrm{T}}\boldsymbol{M}\dot{\boldsymbol{q}}(\theta,t)\mathrm{d}\theta \end{aligned} \tag{3}$$

where, ρ is material density of the element, and

$$\boldsymbol{M} = \int_A \rho r \boldsymbol{\Phi}^{\mathrm{T}}(r,y)\boldsymbol{\Phi}(r,y)\mathrm{d}A, \tag{4}$$

is termed the mass matrix of the element.

The potential energy of the element volume is given by [5, Page 39-40]

$$U = \frac{1}{2}\int_A \boldsymbol{\varepsilon}^{\mathrm{T}}\boldsymbol{D}\boldsymbol{\varepsilon} r\mathrm{d}A\mathrm{d}\theta, \tag{5}$$

where,

$$\boldsymbol{\varepsilon} = (\varepsilon_r, \varepsilon_y, \varepsilon_\theta, \gamma_{ry}, \gamma_{r\theta}, \gamma_{y\theta})^{\mathrm{T}}, \tag{6}$$

is the strain vector, given by

$$\boldsymbol{\varepsilon} = (\frac{\partial u}{\partial r}, \frac{\partial \upsilon}{\partial y}, \frac{u}{r} + \frac{\partial w}{r\partial\theta}, \frac{\partial u}{\partial y} + \frac{\partial \upsilon}{\partial r}, \frac{\partial u}{r\partial\theta} + \frac{\partial w}{\partial r} - \frac{w}{r}, \frac{\partial \upsilon}{r\partial\theta} + \frac{\partial w}{\partial y})^{\mathrm{T}}, \tag{7}$$

and $\boldsymbol{D}$ is the stress-strain matrix, given by

$$\boldsymbol{D} = \frac{E}{(1+\nu)(1-2\nu)}\begin{bmatrix} 1-\nu & \nu & \nu & 0 & 0 & 0 \\ \nu & 1-\nu & \nu & 0 & 0 & 0 \\ \nu & \nu & 1-\nu & 0 & 0 & 0 \\ 0 & 0 & 0 & \frac{1-2\nu}{2} & 0 & 0 \\ 0 & 0 & 0 & 0 & \frac{1-2\nu}{2} & 0 \\ 0 & 0 & 0 & 0 & 0 & \frac{1-2\nu}{2} \end{bmatrix}, \tag{8}$$

where, E is Young's modulus of the material and ν is Poisson ratio. The strain vector may be written as

$$\begin{aligned} \boldsymbol{\varepsilon} &= (\frac{\partial u}{\partial r}, \frac{\partial \upsilon}{\partial y}, \frac{u}{r}, \frac{\partial u}{\partial y} + \frac{\partial \upsilon}{\partial r}, \frac{\partial w}{\partial r} - \frac{w}{r}, \frac{\partial w}{\partial y})^{\mathrm{T}} + (0, 0, \frac{\partial w}{r\partial\theta}, 0, \frac{\partial u}{r\partial\theta}, \frac{\partial \upsilon}{r\partial\theta})^{\mathrm{T}} \\ &= \boldsymbol{B}_1\boldsymbol{v} + \boldsymbol{B}_2\frac{\partial \boldsymbol{v}}{r\partial\theta} \end{aligned}, \tag{9}$$

where,

$$\boldsymbol{B}_1 = \begin{bmatrix} \frac{\partial}{\partial r} & 0 & 0 \\ 0 & \frac{\partial}{\partial y} & 0 \\ \frac{1}{r} & 0 & 0 \\ \frac{\partial}{\partial y} & \frac{\partial}{\partial r} & 0 \\ 0 & 0 & -\frac{1}{r} + \frac{\partial}{\partial r} \\ 0 & 0 & \frac{\partial}{\partial y} \end{bmatrix}, \quad \boldsymbol{B}_2 = \begin{bmatrix} 0 & 0 & 0 \\ 0 & 0 & 0 \\ 0 & 0 & 1 \\ 0 & 0 & 0 \\ 1 & 0 & 0 \\ 0 & 1 & 0 \end{bmatrix}. \tag{10}$$

Thus, Equation (5) becomes

$$\begin{aligned}U &= \frac{1}{2}\int_A (\boldsymbol{B}_1\boldsymbol{v} + \boldsymbol{B}_2 \frac{\partial \boldsymbol{v}}{r\partial\theta})^{\mathrm{T}} \boldsymbol{D}(\boldsymbol{B}_1\boldsymbol{v} + \boldsymbol{B}_2 \frac{\partial \boldsymbol{v}}{r\partial\theta}) r\mathrm{d}A\mathrm{d}\theta \\
&= \frac{1}{2}\int_A \left(\boldsymbol{B}_1\boldsymbol{\Phi}(r,y)\boldsymbol{q}(\theta,t) + \boldsymbol{B}_2\boldsymbol{\Phi}(r,y)\frac{\partial \boldsymbol{q}(\theta,t)}{r\partial\theta}\right)^{\mathrm{T}} \cdot \\
&\qquad \boldsymbol{D}\left(\boldsymbol{B}_1\boldsymbol{\Phi}(r,y)\boldsymbol{q}(\theta,t) + \boldsymbol{B}_2\boldsymbol{\Phi}(r,y)\frac{\partial \boldsymbol{q}(\theta,t)}{r\partial\theta}\right) r\mathrm{d}A\mathrm{d}\theta \\
&= \frac{1}{2}(\boldsymbol{q}(\theta,t))^{\mathrm{T}} \left(\int_A r(\boldsymbol{B}_1\boldsymbol{\Phi}(r,y))^{\mathrm{T}}\boldsymbol{D}\boldsymbol{B}_1\boldsymbol{\Phi}(r,y)\mathrm{d}A\right)\boldsymbol{q}(\theta,t)\mathrm{d}\theta \\
&+ \frac{1}{2}(\boldsymbol{q}(\theta,t))^{\mathrm{T}} \left(\int_A (\boldsymbol{B}_1\boldsymbol{\Phi}(r,y))^{\mathrm{T}}\boldsymbol{D}\boldsymbol{B}_2\boldsymbol{\Phi}(r,y)\mathrm{d}A\right)\frac{\partial \boldsymbol{q}(\theta,t)}{\partial\theta}\mathrm{d}\theta \\
&+ \frac{1}{2}\frac{\partial(\boldsymbol{q}(\theta,t))^{\mathrm{T}}}{\partial\theta} \left(\int_A (\boldsymbol{B}_2\boldsymbol{\Phi}(r,y))^{\mathrm{T}}\boldsymbol{D}\boldsymbol{B}_1\boldsymbol{\Phi}(r,y)\mathrm{d}A\right)\boldsymbol{q}(\theta,t)\mathrm{d}\theta \\
&+ \frac{1}{2}\frac{\partial(\boldsymbol{q}(\theta,t))^{\mathrm{T}}}{\partial\theta} \left(\int_A \frac{1}{r}(\boldsymbol{B}_2\boldsymbol{\Phi}(r,y))^{\mathrm{T}}\boldsymbol{D}\boldsymbol{B}_2\boldsymbol{\Phi}(r,y)\mathrm{d}A\right)\frac{\partial \boldsymbol{q}(\theta,t)}{\partial\theta}\mathrm{d}\theta\end{aligned} \quad . \tag{11}$$

Letting

$$\boldsymbol{K}_0 = \int_A r(\boldsymbol{B}_1\boldsymbol{\Phi}(r,y))^{\mathrm{T}}\boldsymbol{D}\boldsymbol{B}_1\boldsymbol{\Phi}(r,y)\mathrm{d}A, \tag{12}$$

$$\boldsymbol{R}_1 = \int_A (\boldsymbol{B}_1\boldsymbol{\Phi}(r,y))^{\mathrm{T}}\boldsymbol{D}\boldsymbol{B}_2\boldsymbol{\Phi}(r,y)\mathrm{d}A, \tag{13}$$

$$\boldsymbol{R}_2 = \int_A \frac{1}{r}(\boldsymbol{B}_2\boldsymbol{\Phi}(r,y))^{\mathrm{T}}\boldsymbol{D}\boldsymbol{B}_2\boldsymbol{\Phi}(r,y)\mathrm{d}A, \tag{14}$$

then

$$\begin{aligned}U &= \frac{1}{2}(\boldsymbol{q}(\theta,t))^{\mathrm{T}}\boldsymbol{K}_0\boldsymbol{q}(\theta,t)\mathrm{d}\theta + \frac{1}{2}(\boldsymbol{q}(x,t))^{\mathrm{T}}\boldsymbol{R}_1\frac{\partial \boldsymbol{q}(\theta,t)}{\partial\theta}\mathrm{d}\theta \\
&+ \frac{1}{2}\frac{\partial(\boldsymbol{q}(\theta,t))^{\mathrm{T}}}{\partial\theta}\boldsymbol{R}_1^{\mathrm{T}}\boldsymbol{q}(\theta,t)\mathrm{d}\theta + \frac{1}{2}\frac{\partial(\boldsymbol{q}(\theta,t))^{\mathrm{T}}}{\partial\theta}\boldsymbol{R}_2\frac{\partial \boldsymbol{q}(\theta,t)}{\partial\theta}\mathrm{d}\theta\end{aligned} . \tag{15}$$

2.4. Differential equation of motion

According to the Lagrange's equation of the second kind

$$\frac{d}{dt}\frac{\partial T}{\partial \dot{\boldsymbol{q}}} + \frac{\partial U}{\partial \boldsymbol{q}} = \boldsymbol{f}\ , \tag{16}$$

the differential equation of motion of the element volume is given by:

$$\boldsymbol{M}\ddot{\boldsymbol{q}}(\theta,t) + \boldsymbol{K}_0\boldsymbol{q}(\theta,t) + \boldsymbol{R}_1\frac{\partial \boldsymbol{q}(\theta,t)}{\partial\theta} = \boldsymbol{f}_0(\theta,t) + \boldsymbol{f}_1(\theta,t) + \boldsymbol{f}_2(\theta,t), \tag{17}$$

where, $\boldsymbol{f}_0(\theta,t)$ is nodal force vector associated with externally applied loads, $\boldsymbol{f}_1(\theta,t)$ is nodal force vector associated with stresses on the θ and θ+dθ cross-sections of the element volume (see Appendix A), and $\boldsymbol{f}_2(\theta,t)$ is nodal force vector associated with the motion of the *oxyz* system (see Appendix B). Following Appendices A and B, Equation (17) becomes

$$\begin{aligned}&\boldsymbol{M}\ddot{\boldsymbol{q}}(\theta,t) - 2\Omega_y\boldsymbol{G}\dot{\boldsymbol{q}}(\theta,t) + (\boldsymbol{K}_0 - \Omega_y^2\boldsymbol{M}_c)\boldsymbol{q}(\theta,t) + \boldsymbol{K}_1\frac{\partial \boldsymbol{q}(\theta,t)}{\partial\theta} - \boldsymbol{K}_2\frac{\partial^2 \boldsymbol{q}(\theta,t)}{\partial\theta^2} \\
&= \boldsymbol{f}_0(\theta,t) + \Omega_y^2\boldsymbol{h} + \boldsymbol{h}_1\ddot{w}_0(t)\sin(\Omega_y t + \theta) + \boldsymbol{h}_2\ddot{w}_0(t)\cos(\Omega_y t + \theta)\end{aligned} , \tag{18}$$

where, $\boldsymbol{K}_1$ is an anti-symmetric matrix, $\boldsymbol{K}_2$ is an symmetric and positive-definite matrix, and $\boldsymbol{h}$, $\boldsymbol{h}_1$, and $\boldsymbol{h}_2$ are vectors. It is seen that the gyroscopic (the $-2\Omega_y\boldsymbol{G}\dot{\boldsymbol{q}}(\theta,t)$ term) and centrifugal ($-\Omega_y^2\boldsymbol{M}_c\boldsymbol{q}(\theta,t)$ and $\Omega_y^2\boldsymbol{h}$, but the latter causes no vibration) effects caused by the rotation speed appear in the equation. The gyroscopic effect, together with the rotating load, will split a natural frequency of the wheel in stationary into two, one being higher and the other being lower (see Section 4). Since matrix $\boldsymbol{M}_c$ is non-negative, the centrifugal effect will soften the wheel a little bit.

2.5. The assembled finite element model

Equation (18) is for an element (internal forces between elements are not included, since they disappear in the global FE equation). Similar equation can be established for each and every element on the θ-plane. The conventional finite element 'summation' of the element matrices in Equation (18) can be used to obtain the corresponding matrices of the assembled finite element model and thus the global differential equation of motion. This is still represented by Equation (18). In other words, $\boldsymbol{q}(\theta,t)$ is a vector containing all the degrees of freedom on the θ-plane.

2.6. A differential equation governing the vertical motion of the wheel

It can be seen from Equation (18) that the FE equation contains the vertical acceleration, $\ddot{w}_0(t)$, of the mass centre of the wheel, and this is also to be determined. Therefore an extra equation is required. This extra equation may be established by applying the momentum law to the wheel in the vertical direction. This gives

$$\begin{aligned}\sum F_Z(t) = m_{\mathrm{W}}\ddot{w}_0(t) - \Omega_y^2 \int_0^{2\pi} \big(\sin(\Omega_y t+\theta),\, 0,\, \cos(\Omega_y t+\theta)\big)\boldsymbol{S}\boldsymbol{q}(\theta,t)\mathrm{d}\theta \\ + 2\Omega_y \int_0^{2\pi} \big(\cos(\Omega_y t+\theta),\, 0,\, -\sin(\Omega_y t+\theta)\big)\boldsymbol{S}\dot{\boldsymbol{q}}(\theta,t)\mathrm{d}\theta \\ + \int_0^{2\pi} \big(\sin(\Omega_y t+\theta),\, 0,\, \cos(\Omega_y t+\theta)\big)\boldsymbol{S}\ddot{\boldsymbol{q}}(\theta,t)\mathrm{d}\theta\end{aligned} \quad , \qquad (19)$$

where, m_{W} denotes the total mass of the wheel, and $\boldsymbol{S}$ is a $3\times N$ matrix (where, N is the total dofs on the θ-plane), assembled using the FE procedure (in the row direction only) from the following $3\times 3n$ element matrix

$$\boldsymbol{S}_e = \int_A \rho r \boldsymbol{\Phi}(r,y)\mathrm{d}A\,. \qquad (20)$$

Now $\boldsymbol{q}(\theta,t)$ and $\ddot{w}_0(t)$ can be readily determined via Equations (18) and (19).

3. Response of a rotating wheel to a vertical harmonic wheel-rail force

3.1. The associated externally applied nodal force vector

See Figure 1. At position A, the wheel is subject to a vertical (upwards) dynamic load, $P_0\mathrm{e}^{\mathrm{i}\Omega t}$, where, $\mathrm{i}=\sqrt{-1}$, and Ω denotes the angular frequency of the dynamic load. The initial cylindrical coordinates of Point A observed from *oxyz* is $(r_0, y_0, \pi/2)$. At instant t, the wheel has rotated an angle $\Omega_y t$, and the coordinates of Point A become $(r_0, y_0, \pi/2-\Omega_y t)$. The nodal force vector corresponding to this dynamic load is given by

$$\boldsymbol{f}_0(\theta,t) = \boldsymbol{p}_0\delta(\theta+\Omega_y t-\pi/2)\mathrm{e}^{\mathrm{i}\Omega t}\,, \qquad (21)$$

where, $\boldsymbol{p}_0$ is a constant vector, and $\delta(\theta)$ is the delta function of θ.

3.2. Solution for $\boldsymbol{q}(\theta,t)$

Now Equation (18) becomes

$$\begin{aligned}&\boldsymbol{M}\ddot{\boldsymbol{q}}(\theta,t)-2\Omega_y\boldsymbol{G}\dot{\boldsymbol{q}}(\theta,t)+(\boldsymbol{K}_0-\Omega_y^2\boldsymbol{M}_c)\boldsymbol{q}(\theta,t)+\boldsymbol{K}_1\frac{\partial\boldsymbol{q}(\theta,t)}{\partial\theta}-\boldsymbol{K}_2\frac{\partial^2\boldsymbol{q}(\theta,t)}{\partial\theta^2}\\&=\boldsymbol{p}_0\delta(\theta+\Omega_y t-\pi/2)\mathrm{e}^{\mathrm{i}\Omega t}+\Omega_y^2\boldsymbol{h}+\boldsymbol{h}_1\ddot{w}_0(t)\sin(\Omega_y t+\theta)+\boldsymbol{h}_2\ddot{w}_0(t)\cos(\Omega_y t+\theta)\end{aligned}, \quad (22)$$

and Equation (19) becomes

$$\begin{aligned}&m_{\mathrm{W}}\ddot{w}_0(t)-\Omega_y^2\int_0^{2\pi}\big(\sin(\Omega_y t+\theta),0,\cos(\Omega_y t+\theta)\big)\boldsymbol{S}\boldsymbol{q}(\theta,t)\mathrm{d}\theta\\&+2\Omega_y\int_0^{2\pi}\big(\cos(\Omega_y t+\theta),0,-\sin(\Omega_y t+\theta)\big)\boldsymbol{S}\dot{\boldsymbol{q}}(\theta,t)\mathrm{d}\theta\\&+\int_0^{2\pi}\big(\sin(\Omega_y t+\theta),0,\cos(\Omega_y t+\theta)\big)\boldsymbol{S}\ddot{\boldsymbol{q}}(\theta,t)\mathrm{d}\theta=-P_0\mathrm{e}^{\mathrm{i}\Omega t}\end{aligned}. \quad (23)$$

Since $\boldsymbol{q}(\theta,t)$ is periodic function of θ with period 2π, it may be written out

$$\boldsymbol{q}(\theta,t)=\sum_{m=-\infty}^{\infty}\tilde{\boldsymbol{q}}_m(t)\mathrm{e}^{\mathrm{i}m\theta}, \quad (24)$$

and Equation (22) is decomposed into

$$\begin{aligned}&\boldsymbol{M}\ddot{\tilde{\boldsymbol{q}}}_m(t)-2\Omega_y\boldsymbol{G}\dot{\tilde{\boldsymbol{q}}}_m(t)+(\boldsymbol{K}_0-\Omega_y^2\boldsymbol{M}_c)\tilde{\boldsymbol{q}}_m(t)+\mathrm{i}m\boldsymbol{K}_1\tilde{\boldsymbol{q}}_m(t)+m^2\boldsymbol{K}_2\tilde{\boldsymbol{q}}_m(t)\\&=\frac{1}{2\pi}\boldsymbol{p}_0\mathrm{e}^{-\mathrm{i}m\pi/2}\mathrm{e}^{\mathrm{i}(\Omega+m\Omega_y)t}+\varphi(m)\Omega_y^2\boldsymbol{h}\\&+\frac{1}{2\pi}\int_0^{2\pi}\big(\boldsymbol{h}_1\ddot{w}_0(t)\sin(\Omega_y t+\theta)+\boldsymbol{h}_2\ddot{w}_0(t)\cos(\Omega_y t+\theta)\big)\mathrm{e}^{-\mathrm{i}m\theta}\mathrm{d}\theta\end{aligned}, \quad (25)$$

where, $m=-\infty,\cdots,-1,0,1,\cdots,\infty$ and $\varphi(m)$ is a function defined as

$$\varphi(m)=\begin{cases}0, \text{if } m\neq 0;\\1, \text{if } m=0.\end{cases} \quad (26)$$

The integrals in Eq. (25) vanish for $m\neq\pm1$. It can be shown that

$$\int_0^{2\pi}\sin(\Omega_y t+\theta)\mathrm{e}^{\mathrm{i}\theta}\mathrm{d}\theta=\int_0^{2\pi}\frac{\mathrm{e}^{\mathrm{i}(\Omega_y t+\theta)}-\mathrm{e}^{-\mathrm{i}(\Omega_y t+\theta)}}{2\mathrm{i}}\mathrm{e}^{\mathrm{i}\theta}\mathrm{d}\theta=\mathrm{i}\pi\,\mathrm{e}^{-\mathrm{i}\Omega_y t}, \quad (27)$$

$$\int_0^{2\pi}\cos(\Omega_y t+\theta)\mathrm{e}^{\mathrm{i}\theta}\mathrm{d}\theta=\int_0^{2\pi}\frac{\mathrm{e}^{\mathrm{i}(\Omega_y t+\theta)}+\mathrm{e}^{-\mathrm{i}(\Omega_y t+\theta)}}{2}\mathrm{e}^{\mathrm{i}\theta}\mathrm{d}\theta=\pi\mathrm{e}^{-\mathrm{i}\Omega_y t}, \quad (28)$$

$$\int_0^{2\pi}\sin(\Omega_y t+\theta)\mathrm{e}^{-\mathrm{i}\theta}\mathrm{d}\theta=\int_0^{2\pi}\frac{\mathrm{e}^{\mathrm{i}(\Omega_y t+\theta)}-\mathrm{e}^{-\mathrm{i}(\Omega_y t+\theta)}}{2\mathrm{i}}\mathrm{e}^{-\mathrm{i}\theta}\mathrm{d}\theta=-\mathrm{i}\pi\,\mathrm{e}^{\mathrm{i}\Omega_y t}, \quad (29)$$

$$\int_0^{2\pi}\cos(\Omega_y t+\theta)\mathrm{e}^{-\mathrm{i}\theta}\mathrm{d}\theta=\int_0^{2\pi}\frac{\mathrm{e}^{\mathrm{i}(\Omega_y t+\theta)}+\mathrm{e}^{-\mathrm{i}(\Omega_y t+\theta)}}{2}\mathrm{e}^{-\mathrm{i}\theta}\mathrm{d}\theta=\pi\mathrm{e}^{\mathrm{i}\Omega_y t}. \quad (30)$$

Thus, Eq. (25) reduces to

$$\begin{aligned}&\boldsymbol{M}\ddot{\tilde{\boldsymbol{q}}}_{-1}(t)-2\Omega_y\boldsymbol{G}\dot{\tilde{\boldsymbol{q}}}_{-1}(t)+(\boldsymbol{K}_0-\Omega_y^2\boldsymbol{M}_c)\tilde{\boldsymbol{q}}_{-1}(t)-\mathrm{i}\boldsymbol{K}_1\tilde{\boldsymbol{q}}_{-1}(t)+\boldsymbol{K}_2\tilde{\boldsymbol{q}}_{-1}(t)\\&=\frac{\mathrm{i}}{2\pi}\boldsymbol{p}_0\mathrm{e}^{\mathrm{i}(\Omega-\Omega_y)t}+\frac{\mathrm{i}}{2}\boldsymbol{h}_1\ddot{w}_0(t)e^{-\mathrm{i}\Omega_y t}+\frac{1}{2}\boldsymbol{h}_2\ddot{w}_0(t)e^{-\mathrm{i}\Omega_y t}\end{aligned}, \quad (31)$$

$$\begin{aligned}&\boldsymbol{M}\ddot{\tilde{\boldsymbol{q}}}_1(t)-2\Omega_y\boldsymbol{G}\dot{\tilde{\boldsymbol{q}}}_1(t)+(\boldsymbol{K}_0-\Omega_y^2\boldsymbol{M}_c)\tilde{\boldsymbol{q}}_1(t)+\mathrm{i}\boldsymbol{K}_1\tilde{\boldsymbol{q}}_1(t)+\boldsymbol{K}_2\tilde{\boldsymbol{q}}_1(t)\\&=\frac{-\mathrm{i}}{2\pi}\boldsymbol{p}_0\mathrm{e}^{\mathrm{i}(\Omega+\Omega_y)t}-\frac{\mathrm{i}}{2}\boldsymbol{h}_1\ddot{w}_0(t)\mathrm{e}^{\mathrm{i}\Omega_y t}+\frac{1}{2}\boldsymbol{h}_2\ddot{w}_0(t)\mathrm{e}^{\mathrm{i}\Omega_y t}\end{aligned}, \tag{32}$$

$$\begin{aligned}&\boldsymbol{M}\ddot{\tilde{\boldsymbol{q}}}_m(t)-2\Omega_y\boldsymbol{G}\dot{\tilde{\boldsymbol{q}}}_m(t)+(\boldsymbol{K}_0-\Omega_y^2\boldsymbol{M}_c)\tilde{\boldsymbol{q}}_m(t)+\mathrm{i}m\boldsymbol{K}_1\tilde{\boldsymbol{q}}_m(t)+m^2\boldsymbol{K}_2\tilde{\boldsymbol{q}}_m(t)\\&=\frac{1}{2\pi}\boldsymbol{p}_0\mathrm{e}^{-\mathrm{i}m\pi/2}\mathrm{e}^{\mathrm{i}(\Omega+m\Omega_y)t},\quad(m\neq\pm1)\end{aligned}. \tag{33}$$

The steady state solution of Eq. (33) is given by

$$\begin{aligned}\tilde{\boldsymbol{q}}_m(t)&=\hat{\boldsymbol{q}}_m\mathrm{e}^{\mathrm{i}(\Omega+m\Omega_y)t}\\&=\frac{1}{2\pi}\left(\boldsymbol{K}_0-\Omega_y^2\boldsymbol{M}_c+\mathrm{i}m\boldsymbol{K}_1+m^2\boldsymbol{K}_2-2\mathrm{i}\Omega_y(\Omega+m\Omega_y)\boldsymbol{G}-(\Omega+m\Omega_y)^2\boldsymbol{M}\right)^{-1}\\&\quad\times\boldsymbol{p}_0\mathrm{e}^{-\mathrm{i}m\pi/2}\mathrm{e}^{\mathrm{i}(\Omega+m\Omega_y)t}\end{aligned}. \tag{34}$$

Now insertion of Equation (24) into Equation (23), and according to Equations (27)-(30), gives

$$\begin{aligned}&m_{\mathrm{W}}\ddot{w}_0(t)-\Omega_y^2(\mathrm{i}\pi,0,\ \pi)\boldsymbol{S}\tilde{\boldsymbol{q}}_1(t)\,\mathrm{e}^{-\mathrm{i}\Omega_y t}-\Omega_y^2(-\mathrm{i}\pi,0,\ \pi)\boldsymbol{S}\tilde{\boldsymbol{q}}_{-1}(t)\,\mathrm{e}^{\mathrm{i}\Omega_y t}\\&+2\Omega_y(\pi,0,\ -\mathrm{i}\pi)\boldsymbol{S}\dot{\tilde{\boldsymbol{q}}}_1(t)\,\mathrm{e}^{-\mathrm{i}\Omega_y t}+2\Omega_y(\pi,0,\ \mathrm{i}\pi)\boldsymbol{S}\dot{\tilde{\boldsymbol{q}}}_{-1}(t)\,\mathrm{e}^{\mathrm{i}\Omega_y t}\\&+(\mathrm{i}\pi,0,\ \pi)\boldsymbol{S}\ddot{\tilde{\boldsymbol{q}}}_1(t)\,\mathrm{e}^{-\mathrm{i}\Omega_y t}+(-\mathrm{i}\pi,0,\ \pi)\boldsymbol{S}\ddot{\tilde{\boldsymbol{q}}}_{-1}(t)\,\mathrm{e}^{\mathrm{i}\Omega_y t}=-P_0\mathrm{e}^{\mathrm{i}\Omega t}\end{aligned}. \tag{35}$$

From Equations (31), (32) and (35), $\ddot{w}_0(t)$, $\tilde{\boldsymbol{q}}_{-1}(t)$ and $\tilde{\boldsymbol{q}}_1(t)$ may be worked out by letting

$$w_0(t)=\hat{w}_0\mathrm{e}^{\mathrm{i}\Omega t},\quad\tilde{\boldsymbol{q}}_{-1}(t)=\hat{\boldsymbol{q}}_{-1}\mathrm{e}^{\mathrm{i}(\Omega-\Omega_y)t},\quad\tilde{\boldsymbol{q}}_1(t)=\hat{\boldsymbol{q}}_1\mathrm{e}^{\mathrm{i}(\Omega+\Omega_y)t}. \tag{36}$$

Equations (34 and (36) show that,

$$\tilde{\boldsymbol{q}}_m(t)=\hat{\boldsymbol{q}}_m\mathrm{e}^{\mathrm{i}(\Omega+m\Omega_y)t},\ (m=-\infty,\cdots,-1,0,1,\cdots,\infty), \tag{37}$$

and Equation (24) becomes

$$\boldsymbol{q}(\theta,t)=\sum_{m=-\infty}^{\infty}\hat{\boldsymbol{q}}_m\mathrm{e}^{\mathrm{i}[m\theta+(\Omega+m\Omega_y)t]}. \tag{38}$$

3.3. Displacement defined for an observation point fixed in the moving inertial reference frame OXYZ

A cross-section containing the wheel axis and stationary with the moving inertial reference frame *OXYZ* may be defined by an angle, α, measured from the horizontal plane. The displacement, observed from *OXYZ*, of the cross-section consists of two parts. The first part is the vertical displacement of the wheel axis, which is harmonic at the wheel-rail force frequency, as indicated in Equation (36). For the second part at that cross-section, the radial, axial and circumferential displacement components are given by setting $\theta=\alpha-\Omega_y t$ in Equation (38)

$$\boldsymbol{w}(t)=\sum_{m=-\infty}^{\infty}\hat{\boldsymbol{q}}_m\mathrm{e}^{\mathrm{i}(\Omega+m\Omega_y)t}\mathrm{e}^{\mathrm{i}m(\alpha-\Omega_y t)}=\left(\sum_{m=-\infty}^{\infty}\hat{\boldsymbol{q}}_m\mathrm{e}^{\mathrm{i}m\alpha}\right)\mathrm{e}^{\mathrm{i}\Omega t}. \tag{39}$$

Equation (39) shows that the displacement of the cross-section, observed from the moving inertial reference frame *OXYZ*, is harmonic at the same frequency as the wheel-rail force, and the amplitude, as a periodic function of the circumferential angle α, is decomposed into an infinite number of spatial harmonics. This may be utilised to simplify the calculation of sound radiation from the wheel.

3.4. Vertical displacement of the wheel at the wheel-rail contact point

The vertical displacement of the wheel at the wheel-rail contact point, if observed from the moving reference frame *OXYZ*, is given by (directed downwards) setting $\theta=\pi/2-\Omega_y t$ in Eq. (38) and combining Eq. (36)

$$W(t) = \hat{w}_0 \mathrm{e}^{\mathrm{i}\Omega t} + \sum_{m=-\infty}^{\infty} \hat{\varphi}_m \mathrm{e}^{\mathrm{i}(\Omega + m\Omega_y)t} \mathrm{e}^{\mathrm{i}m(\frac{\pi}{2} - \Omega_y t)} = \left(\hat{w}_0 + \sum_{m=-\infty}^{\infty} \hat{\varphi}_m \mathrm{e}^{\mathrm{i}m\frac{\pi}{2}} \right) \mathrm{e}^{\mathrm{i}\Omega t}, \tag{40}$$

where, $\hat{\varphi}_m$ denotes the component in $\hat{\boldsymbol{q}}_m$ corresponding to the radial displacement of the wheel-rail contact point. It can be seen that the vertical displacement at the wheel-rail contact point is harmonic at the same frequency as the wheel-rail force. Therefore the Fourier series approach to dealing wheel-rail interactions [6] will still be applicable even the rotation of the wheels are taken into account.

4. Results

In this section, vertical responses of a high-speed train wheel subject to a unit vertical harmonic wheel-rail force are calculated for the wheel-rail contact point as well as for the wheel axis, using equations derived in previous sections. The 2D mesh of the wheel is shown in Figure 3. Material parameters are density 7850kg/m^3, Young's modulus 210GPa, Poisson ratio 0.30, and loss factor 0.005. The rolling radius of the wheel is 0.46m.

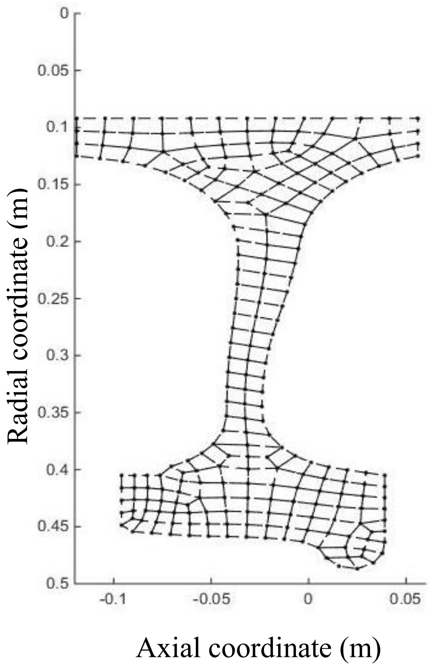

Figure 3. Finite element mesh of a high-speed wheel.

The vertical receptance of the wheel at the wheel-rail contact point is shown in Figure 4 with solid lines for the wheel not in rotation and dashed lines for the wheel travelling at 300km/h (83m/s) or rotating at 29 Hz. The frequency resolution is 10Hz.

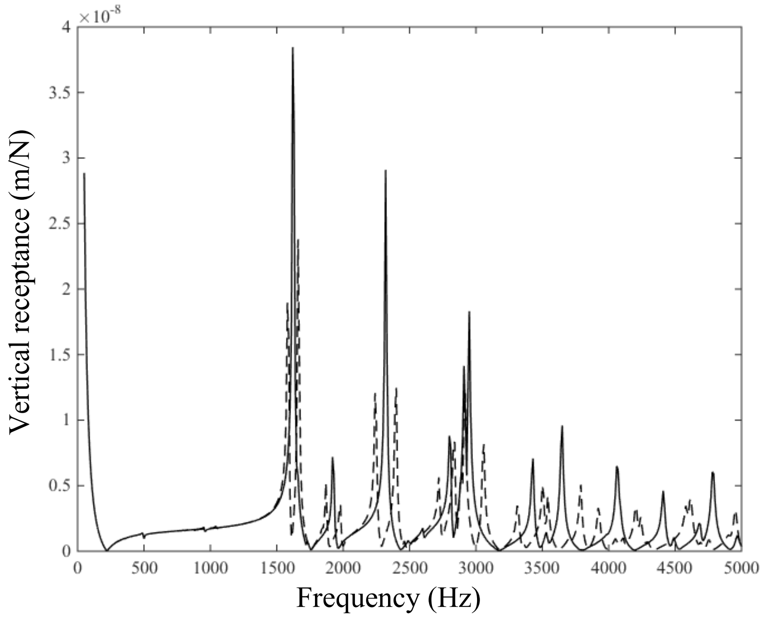

Figure 4. Vertical receptance of the wheel at the wheel-rail contact point. ——, wheel not in rotation; – – –, wheel travelling at 300km/h or rotating at 29 Hz.

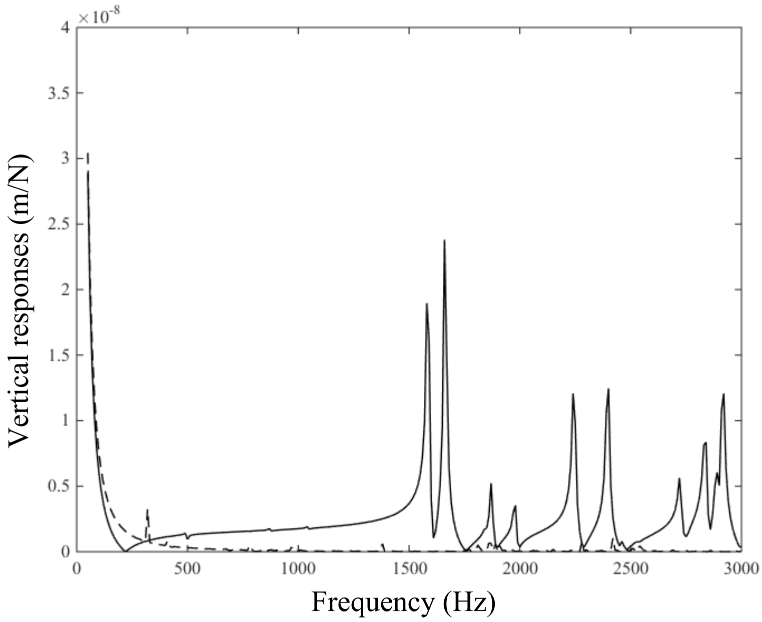

Figure 5. Vertical responses of the wheel rotating at 300km/h. ——, at the wheel-rail contact point; – – –, at the wheel axis.

It can be seen that resonances occur for frequency higher than 1500 Hz. The rotation speed splits a peak at a natural frequency into two peaks. This is the combined result of the gyroscopic effect of the wheel rotation and the rotating of the wheel-rail force along the periphery of the wheel. Separation of the peaks due to the rotating force is given by $2m\Omega_y$, depending not only on the wheel spinning speed Ω_y, but also on the circumferential order, m, to which the original frequency is corresponding.

Two other observations can be made according to Figure 4; the first is that the amplitudes of the peaks are much reduced by the wheel speed, and the second is that, for frequencies well below the first resonance frequency, there is no difference between a stationary wheel and a travelling wheel.

Comparison between the vertical response of the wheel at the wheel-rail contact point (solid line) and that at the wheel axis is shown in Figure 5. The wheel is rotating at 300km/h. It is seen that, the response at the wheel axis is almost identical to the response of the wheel as a rigid body apart from few small peaks. It can also be seen that, below about 250Hz, the difference in response between the wheel-rail contact point and the wheel axis is very small, indicating that the wheel behaves like a rigid body.

The gyroscopic effect of wheel rotation is demonstrated in Figure 6. For easy comparison, the original receptance is also shown in this figure in solid lines. It can be seen that, by setting $\boldsymbol{G} = 0$ in Equation (18), the splitting of a peak is slightly wider. The splitting of a peak is just caused by the load which rotates around the wheel when $\boldsymbol{G} = 0$. The heights of the peaks do not change significantly by setting $\boldsymbol{G} = 0$. In other words, the gyroscopic effect of wheel rotation is insignificant.

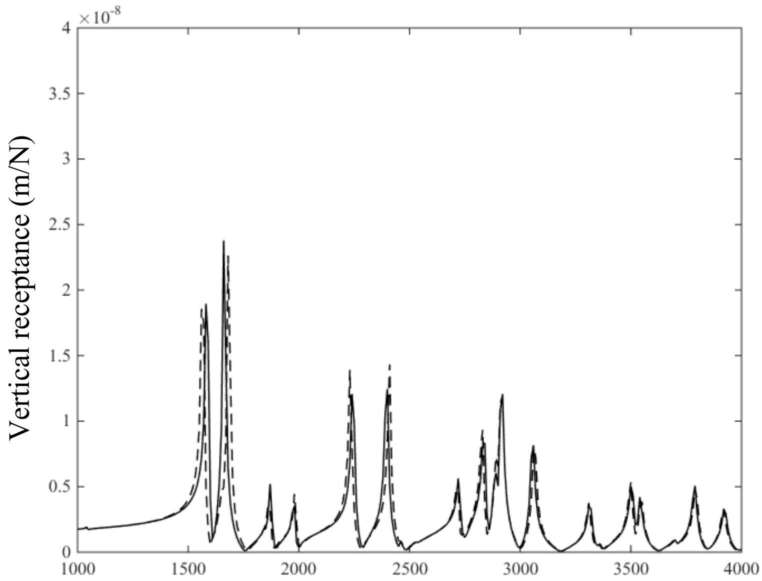

Figure 6. Vertical receptance at the wheel-rail contact point of the wheel travelling at 300km/h or rotating at 29 Hz. ——, including all the rotation effects; — — —, excluding the gyroscopic effect by setting $\boldsymbol{G} = 0$ in Equation (18).

The centrifugal effect of wheel rotation is investigated by setting $\boldsymbol{Mc} = 0$ in Equation (18). Results show that the centrifugal effect is very insignificant.

5. Conclusions

In this paper, by making use of axial symmetry, a special finite element scheme, combined with application of the momentum law to the wheel, is developed for responses of a train wheel subject to a vertical and harmonic wheel-rail force. This FE scheme only requires a 2D mesh over a cross-section containing the wheel axis but includes all the effects induced by wheel rotation. Unknowns include vertical displacement of the wheel axis, and nodal displacements, as a function of the cross-section angle θ, of the cross-section observed from the rotating wheel. Since the nodal displacements are a periodic function of θ, they can be decomposed, using Fourier series, into a number of components at different circumferential orders. The derived FE equation is solved for each circumferential order. The sum of responses at all circumferential orders gives the actual response of the wheel observed from the rotating wheel.

In case of a vertical harmonic wheel-rail force, it is shown that:

(1) The vertical vibration of the wheel axis is harmonic at the same frequency as the wheel-rail force;

(2) The displacement of the wheel, if observed from the moving inertial reference frame *OXYZ*, e.g. the vertical displacement of the wheel at the wheel-rail contact point, is also harmonic at the same frequency as the wheel-rail force;

(3) Below about 250Hz, the vertical receptance of the wheel at the wheel-rail contact point is very close to that of the wheel as a rigid body. Resonances occur for frequency higher than 1500 Hz.

(4) The rotation speed splits a natural frequency into two. The amplitudes of the peaks of the vertical receptance of the wheel at the wheel-rail contact point are much reduced by the wheel speed if compared with those without wheel rotation;

(5) The effects of wheel rotation listed in (4) are caused mainly by the rotating of the wheel-rail force along the periphery of the wheel, and the gyroscopic and centrifugal effects are insignificant.

Acknowledgement
This work is funded by China Railway under Project 2015Z003-B, and National Natural Science Foundation of China under Project U1434201.

Appendix A. Virtual work done by stresses on the θ and θ+dθ cross-sections of the element volume

By referring to Figure A.1, it is seen that the virtual work done by stresses on the θ and θ+dθ cross-sections of the element volume due to a virtual displacement (vector), $\delta\boldsymbol{q}(\theta,t)$, is given by

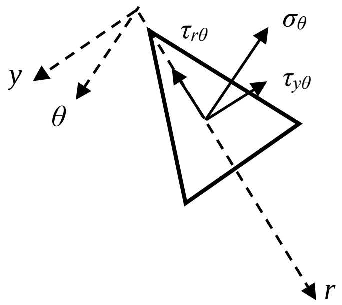

Figure A1. Stresses on the θ-plane.

$$\delta W = \frac{\partial}{\partial\theta}\int_A [\tau_{r\theta}\delta u + \tau_{y\theta}\delta\upsilon + \sigma_\theta \delta w]\mathrm{d}A\mathrm{d}\theta\ . \tag{A.1}$$

According to Hooke's law and Equation (7),

$$\tau_{r\theta} = G\gamma_{r\theta} = \frac{E}{2(1+\nu)}\left(\frac{\partial u}{r\partial\theta} + \frac{\partial w}{\partial r} - \frac{w}{r}\right), \tag{A.2}$$

$$\tau_{y\theta} = G\gamma_{y\theta} = \frac{E}{2(1+\nu)}\left(\frac{\partial\upsilon}{r\partial\theta} + \frac{\partial w}{\partial y}\right), \tag{A.3}$$

$$\sigma_\theta = \frac{E}{(1+\nu)(1-2\nu)}\left(\nu(\frac{\partial u}{\partial r} + \frac{\partial\upsilon}{\partial y}) + (1-\nu)\frac{u}{r} + (1-\nu)\frac{\partial w}{r\partial\theta}\right), \tag{A.4}$$

and if define

$$\boldsymbol{B}_3 = \frac{E}{(1+\nu)(1-2\nu)}\begin{bmatrix} 0 & 0 & \frac{1-2\nu}{2}(-\frac{1}{r}+\frac{\partial}{\partial r}) \\ 0 & 0 & \frac{1-2\nu}{2}\frac{\partial}{\partial y} \\ \frac{1-\nu}{r}+\nu\frac{\partial}{\partial r} & \nu\frac{\partial}{\partial y} & 0 \end{bmatrix}, \tag{A.5}$$

$$\boldsymbol{B}_4 = \frac{E}{(1+\nu)(1-2\nu)}\begin{bmatrix} \frac{1-2\nu}{2} & 0 & 0 \\ 0 & \frac{1-2\nu}{2} & 0 \\ 0 & 0 & 1-\nu \end{bmatrix}, \tag{A.6}$$

then Equation (A.1) becomes

$$\begin{aligned} \delta W &= \frac{\partial}{\partial\theta}\int_A \delta(\boldsymbol{q}(\theta,t))^{\mathrm{T}}(\boldsymbol{\Phi}(r,y))^{\mathrm{T}}\left((\boldsymbol{B}_3+\boldsymbol{B}_4\frac{\partial}{r\partial\theta})\boldsymbol{\Phi}(r,y)\boldsymbol{q}(\theta,t)\right)\mathrm{d}A\mathrm{d}\theta \\ &= \int_A \delta(\boldsymbol{q}(\theta,t))^{\mathrm{T}}(\boldsymbol{\Phi}(r,y))^{\mathrm{T}}\left((\boldsymbol{B}_3\boldsymbol{\Phi}(r,y)\frac{\partial\boldsymbol{q}(\theta,t)}{\partial\theta}+\boldsymbol{B}_4\boldsymbol{\Phi}(r,y)\frac{\partial^2\boldsymbol{q}(\theta,t)}{r\partial\theta^2}\right)\mathrm{d}A\mathrm{d}\theta \\ &= \delta(\boldsymbol{q}(\theta,t))^{\mathrm{T}}\left(\int_A(\boldsymbol{\Phi}(r,y))^{\mathrm{T}}\boldsymbol{B}_3\boldsymbol{\Phi}(r,y)\mathrm{d}A\right)\frac{\partial\boldsymbol{q}(\theta,t)}{\partial\theta}\mathrm{d}\theta \\ &\quad+\delta(\boldsymbol{q}(\theta,t))^{\mathrm{T}}\left(\int_A\frac{1}{r}(\boldsymbol{\Phi}(r,y))^{\mathrm{T}}\boldsymbol{B}_4\boldsymbol{\Phi}(r,y)\mathrm{d}A\right)\frac{\partial^2\boldsymbol{q}(\theta,t)}{\partial\theta^2}\mathrm{d}\theta \end{aligned}, \tag{A.7}$$

i.e.

$$\delta W = \delta(\boldsymbol{q}(\theta,t))^{\mathrm{T}}\boldsymbol{R}_3\frac{\partial\boldsymbol{q}(\theta,t)}{\partial\theta}\mathrm{d}\theta+\delta(\boldsymbol{q}(\theta,t))^{\mathrm{T}}\boldsymbol{R}_4\frac{\partial^2\boldsymbol{q}(\theta,t)}{\partial\theta^2}\mathrm{d}\theta, \tag{A.8}$$

where,

$$\boldsymbol{R}_3 = \int_A(\boldsymbol{\Phi}(r,y))^{\mathrm{T}}\boldsymbol{B}_3\boldsymbol{\Phi}(r,y)\mathrm{d}A, \tag{A.9}$$

$$\boldsymbol{R}_4 = \int_A\frac{1}{r}(\boldsymbol{\Phi}(r,y))^{\mathrm{T}}\boldsymbol{B}_4\boldsymbol{\Phi}(r,y)\mathrm{d}A. \tag{A.10}$$

Therefore the associated generalised force vector is given by (dθ is dropped)

$$\boldsymbol{f}_1(\theta,t) = \boldsymbol{R}_3\frac{\partial\boldsymbol{q}(\theta,t)}{\partial\theta}+\boldsymbol{R}_4\frac{\partial^2\boldsymbol{q}(\theta,t)}{\partial\theta^2}. \tag{A.11}$$

Appendix B. Virtual work done by convection inertial forces of the element volume

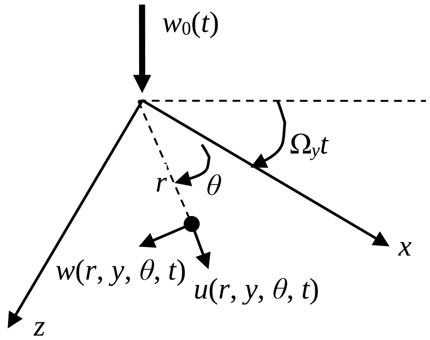

Figure B1. Various displacements.

The r- (radial), y- (axial) and θ-(circumferential) components of the convection acceleration associated with the vertical motion of the y-axis are given by (see Figure B1)

$$\boldsymbol{a}_{c0} = \begin{Bmatrix} \ddot{w}_0(t)\sin(\Omega_y t+\theta) \\ 0 \\ \ddot{w}_0(t)\cos(\Omega_y t+\theta) \end{Bmatrix}. \tag{B.1}$$

The convection acceleration associated with the rotation of the wheel (centrifugal acceleration) is given by

$$\boldsymbol{a}_{c1} = \begin{Bmatrix} -\Omega_y^2(r+u) \\ 0 \\ -\Omega_y^2 w \end{Bmatrix}, \tag{B.2}$$

and those associated with Coriolis acceleration is given by

$$\boldsymbol{a}_{c2} = \begin{Bmatrix} -2\Omega_y \dot{w} \\ 0 \\ 2\Omega_y \dot{u} \end{Bmatrix}. \tag{B.3}$$

Virtual work done by inertial forces associated with these accelerations is given by

$$\begin{aligned} \delta W &= -\int_A \rho(\delta u, \delta \upsilon, \delta w)^{\mathrm{T}}(\boldsymbol{a}_{c1}+\boldsymbol{a}_{c2}+\boldsymbol{a}_{c3}) r\mathrm{d}A\mathrm{d}\theta \\ &= -\int_A \rho(\delta\boldsymbol{q})^{\mathrm{T}}(\boldsymbol{\Phi}(r,y))^{\mathrm{T}}\left(\begin{Bmatrix} \ddot{w}_0(t)\sin(\Omega_y t+\theta) \\ 0 \\ \ddot{w}_0(t)\cos(\Omega_y t+\theta) \end{Bmatrix} + \begin{Bmatrix} -\Omega_y^2(r+u) \\ 0 \\ -\Omega_y^2 w \end{Bmatrix} + \begin{Bmatrix} -2\Omega_y \dot{w} \\ 0 \\ 2\Omega_y \dot{u} \end{Bmatrix}\right) r\mathrm{d}A\mathrm{d}\theta, \end{aligned} \tag{B.4}$$

$$\begin{aligned} \delta W = &-(\delta\boldsymbol{q})^{\mathrm{T}}\left(\int_A \rho(\boldsymbol{\Phi}(r,y))^{\mathrm{T}} r\mathrm{d}A\right)\begin{Bmatrix} \ddot{w}_0(t)\sin(\Omega_y t+\theta) \\ 0 \\ \ddot{w}_0(t)\cos(\Omega_y t+\theta) \end{Bmatrix}\mathrm{d}\theta \\ &+(\delta\boldsymbol{q})^{\mathrm{T}}\int_A \rho(\boldsymbol{\Phi}(r,y))^{\mathrm{T}}\begin{Bmatrix} \Omega_y^2 r \\ 0 \\ 0 \end{Bmatrix} r\mathrm{d}A\mathrm{d}\theta \\ &+(\delta\boldsymbol{q})^{\mathrm{T}}\left(\int_A \rho(\boldsymbol{\Phi}(r,y))^{\mathrm{T}}\begin{bmatrix} \Omega_y^2 & 0 & 0 \\ 0 & 0 & 0 \\ 0 & 0 & \Omega_y^2 \end{bmatrix}\boldsymbol{\Phi}(r,y) r\mathrm{d}A\right)\boldsymbol{q}(\theta,t)\mathrm{d}\theta \\ &-(\delta\boldsymbol{q})^{\mathrm{T}}\left(\int_A \rho(\boldsymbol{\Phi}(r,y))^{\mathrm{T}}\begin{bmatrix} 0 & 0 & -2\Omega_y \\ 0 & 0 & 0 \\ 2\Omega_y & 0 & 0 \end{bmatrix}\boldsymbol{\Phi}(r,y) r\mathrm{d}A\right)\dot{\boldsymbol{q}}(\theta,t)\mathrm{d}\theta \end{aligned}. \tag{B.5}$$

Therefore, the associated generalised force vector is given by

$$\boldsymbol{f}_2(\theta,t) = \Omega_y^2\boldsymbol{h} + \Omega_y^2\boldsymbol{M}_c\boldsymbol{q}(\theta,t) + 2\Omega_y\boldsymbol{G}\dot{\boldsymbol{q}}(\theta,t) + \boldsymbol{h}_1\ddot{w}_0(t)\sin(\Omega_y t+\theta) + \boldsymbol{h}_2\ddot{w}_0(t)\cos(\Omega_y t+\theta), \tag{B.6}$$

where,

$$\boldsymbol{h} = \left(\int_A \rho r^2 (\boldsymbol{\Phi}(r,y))^{\mathrm{T}} \mathrm{d}A\right)\begin{Bmatrix}1\\0\\0\end{Bmatrix}, \text{ (order of } 3n\times 1\text{)}, \tag{B.7}$$

$$\boldsymbol{h}_1 = -\left(\int_A \rho r (\boldsymbol{\Phi}(r,y))^{\mathrm{T}} \mathrm{d}A\right)\begin{Bmatrix}1\\0\\0\end{Bmatrix}, \text{ (order of } 3n\times 1\text{)}, \tag{B.8}$$

$$\boldsymbol{h}_2 = -\left(\int_A \rho r (\boldsymbol{\Phi}(r,y))^{\mathrm{T}} \mathrm{d}A\right)\begin{Bmatrix}0\\0\\1\end{Bmatrix}, \text{ (order of } 3n\times 1\text{)}, \tag{B.9}$$

$$\boldsymbol{M}_c = \int_A \rho r (\boldsymbol{\Phi}(r,y))^{\mathrm{T}} \begin{bmatrix}1&0&0\\0&0&0\\0&0&1\end{bmatrix} \boldsymbol{\Phi}(r,y)\mathrm{d}A, \tag{B.10}$$

$$\boldsymbol{G} = \int_A \rho r (\boldsymbol{\Phi}(r,y))^{\mathrm{T}} \begin{bmatrix}0&0&1\\0&0&0\\-1&0&0\end{bmatrix} \boldsymbol{\Phi}(r,y)\mathrm{d}A. \tag{B.11}$$

References

[1] Thompson D J 1993 Wheel-rail noise generation, Part V: inclusion of wheel rotation *Journal of Sound and Vibration* **161** 467-482.

[2] Thompson D J, Jones C J C 2000 A review of the modelling of wheel/rail noise generation *Journal of Sound and Vibration* **231** 519-536.

[3] Fayos J, Baeza L, Denia F D, Tarancón J E 2007 An Eulerian coordinate-based method for analyzing the structural vibrations of a solid of revolution rotating about its main axis *Journal of Sound and Vibration* **306** 618–635.

[4] Baeza L, Vila P, Xie G, Iwnicki S D 2011 Prediction of rail corrugation using a rotating flexible wheelset coupled with a flexible track model and a non-Hertzian/non-steady contact model *Journal of Sound and Vibration* **330** 4493–4507.

[5] Petyt M 1990 *Introduction to finite element vibration analysis* (New York: Cambridge University Press).

[6] Sheng X, Li M, Jones C J C, Thompson D J 2007 Using the Fourier series approach to study interactions between moving wheels and a periodically supported rail *Journal of Sound and Vibration* **303** 873-984.